Unified semiclassical approximation for Bose-Einstein condensates: Application to a BEC in an optical potential

Y. B. Band and I. Towers*
Department of Chemistry, Ben-Gurion University of the Negev, 84105 Beer-Sheva, Israel

B. A. Malomed
Department of Interdisciplinary Studies, Faculty of Engineering, Tel Aviv University, Tel Aviv 69978, Israel
(Received 31 July 2002; published 7 February 2003)

We present semiclassical descriptions of Bose-Einstein condensates for configurations with spatial symmetry, e.g., cylindrical symmetry, and without any symmetry. The description of the cylindrical case is quasi-one-dimensional (Q1D), in the sense that one only needs to solve an effective 1D nonlinear Schrödinger equation, but the solution incorporates 3D aspects of the problem, as a result of which the 1D equation is supplemented by a noncanonical (quartic) normalization condition. The solution in classically allowed regions is matched onto that in classically forbidden regions by a connection formula that properly accounts for the nonlinear mean-field interaction. Special cases for vortex solutions are treated too. Comparisons of the Q1D solution with the full 3D and Thomas-Fermi ones are presented, and conditions for the applicability of the effective low-dimensional equations are obtained.

DOI: 10.1103/PhysRevA.67.023602 PACS number(s): 03.75.Kk, 67.90.+z, 71.35.Lk

I. INTRODUCTION

Simple models of Bose-Einstein condensates (BECs) have been very useful for understanding their physics. For example, in the mean-field approximation for BECs with repulsive atom-atom interactions, in regions where the local density is large enough and the mean-field (nonlinear) term in the Gross-Pitaevskii equation (GPE) is much larger than the kinetic-energy term, the Thomas-Fermi (TF) approximation offers such a simplified description for the ground state of a BEC in a stationary potential [1]. However, in classically forbidden regions of the coordinate space, the density is low and the TF approximation is invalid. It is necessary to match the TF approximation in the region of high density to a description valid near the boundaries of the classically allowed motion and inside the classically forbidden region for a given external potential. For dynamic situations, some simple approximations exist for time-dependent harmonic potentials [2,3]. It would be very useful to have a simple effective one-dimensional (1D) approximation that properly accounts for the 3D character of a BEC, for both static and dynamic problems in configurations with spatial symmetry, such as a BEC in a cylindrically symmetric potential (e.g., a harmonic trap with cylindrical symmetry, with or without an optical potential that varies in space along the symmetry axis of the harmonic potential, see a detailed formulation of the model below in Sec. II). Pedri *et al.* developed a treatment of this kind [4]. Another contribution was made in Ref. [5], which aimed at a derivation of an effectively one-dimensional (1D) GPE relevant for the description of a 3D BEC by means of the variational approximation. The 1D wave function derived in Ref. [5] was defined so that it has the same density distribution along the symmetry axis of the system as that which could be obtained by integrating the distribution produced by the full 3D wave function in the transverse plane. In the transverse direction, the ansatz adopted in Ref. [5] assumed a Gaussian distribution. As a result, a nonpolynomial GPE was derived in that work. It was used recently [6] to describe macroscopic tunneling in a double-well potential subject to rapid temporal modulation.

Here we develop an approach that differs from the treatments of Refs. [4,5] in several ways. In our treatment in Sec. III, regions of physical space in which the density is sufficient for the application of the mean-field approximation, and those in which the density is low, are treated completely differently. In Sec. IV, we develop a connection (crossover) formula for the wave function in these regions, in analogy with the commonly known formulas between classically allowed and forbidden regions in ordinary quantum mechanics [7] (the difference from the connection formula in quantum mechanics is due to the fact that the GPE is a nonlinear equation). A WKB approximation for the nonlinear Schrödinger equation in an external potential, uniformly valid in classically allowed and forbidden regions, was recently proposed in Ref. [8], but that approximation does not produce the connection formula.

In Sec. III we develop an effectively 1D treatment of the dynamics with the cylindrical symmetry. In order to reduce the 3D equation to a 1D form, we do not assume a Gaussian distribution in the transverse direction, which is an essential difference from the approach adopted in Refs. [4,5]. Instead, we directly use the TF approximation in 3D. An estimate for the applicability of our method (which relies upon the neglect of the transverse part of the kinetic energy in the GPE) for the case of a cigar-shaped BEC is given by

$$4\pi N a_0 \gg L, \tag{1}$$

where N is the number of atoms, a_0 is the s-wave scattering length, and L is the length of the cigar-shaped configuration. As the longitudinal length and number of atoms are not independent parameters, the value of L to be substituted into Eq. (1) is a function of N, which is to be determined for a

*Present address: Department of Interdisciplinary Studies, Faculty of Engineering, Tel-Aviv University, Tel-Aviv 69978, Israel.

specific potential. Condition (1) may be easily met in situations relevant to experiment (see, for instance, an example given in Sec. VIII below).

If, nevertheless, the condition (1) is not met, the treatment developed in Refs. [4,5] may apply. It should also be mentioned that the approach proposed in Ref. [5] is applicable in an essentially wider parametric range if one is interested in the profile of the condensate density along the cylindrical axis, integrated in the transverse plane [see Eq. (11) in Ref. [5], which demonstrates that the profile directly following from a high-density approximation applied to the above-mentioned nonpolynomial GPE is fairly close to that produced by the TF approximation applied directly to the underlying 3D GPE].

Here, in the classically allowed region, the full 3D GPE is reduced to a 1D equation. However, a drastic difference from the naive 1D description is that the solution to our 1D equation is subject to a *noncanonical* (nonquadratic) normalization condition [see Eq. (16)], which is derived from the canonical normalization for the 3D wave function. As a physically relevant application of the general method, we calculate the quantum-mechanical distribution of values of the longitudinal momentum in a cigar-shaped BEC in Sec. V. This distribution also has a noncanonical form in comparison with ordinary quantum mechanics in 1D. In Sec. VI we generalize the approach to treat the case of a BEC with vorticity; in this case, the effective 1D normalization condition takes on a still more involved form [see Eq. (57)].

We also develop a generalization of our approach for a pancake-shaped condensate, even when the cylindrical symmetry is broken by an external potential, so that the effective equation is 2D, see Sec. VII below. In that case, the applicability condition for our method takes a form different from Eq. (1),

$$\frac{\hbar}{m\omega_\perp}(4\pi a_0 N)^2 \gg R^4, \tag{2}$$

where m is the atom mass, $\omega_\perp$ is the frequency corresponding to the confining potential in the transverse direction, and R is the radius of the pancake. Condition (2) is more restrictive than Eq. (1), but it can also be met in experimentally relevant situations, as is described below [as well as in the case of Eq. (1), the radius and number of atoms, to be substituted into Eq. (2), are not independent parameters, a relation between them being determined by the potential relief in the plane of the pancake]. Finally, the pancake wave function is subject to another noncanonical normalization, see Eq. (60) below.

In Sec. VIII we provide numerical examples that compare our method with full 3D calculations for a BEC in static potentials and for dynamics of a BEC in the presence of a time-varying external potential. The comparison demonstrates the validity of the approach developed in the present work.

II. A MODEL WITH CYLINDRICAL SYMMETRY

We begin by defining the systems of interest to us in the context of a cylindrically symmetric model problem. To this end, we consider a BEC in an array of optical traps, in the presence of the gravitational field and large-size magnetic trap in the form of a parabolic potential induced by the interaction of the magnetic moment of atoms with an external static magnetic field. The static magnetic-trap potential is

$$V_M(\mathbf{r}) = \tfrac{1}{2}m[\omega_z^2 z^2 + \omega_\perp^2(x^2+y^2)], \tag{3}$$

where m is the atomic mass. The optical potential is produced by light beams with identical linear polarizations, whose propagation directions lie in a plane containing the z axis, forming angles $\theta/2$ and $\pi-\theta/2$ with it ($\theta=0$ corresponds to two beams counterpropagating in the $\pm z$ direction). Interference between these fields produces a standing-wave potential along the z direction, whose amplitude is proportional to the intensity of light. It is assumed that the intensity is initially zero and gradually increases with time, hence the light-induced potential experienced by atoms in the BEC is

$$V_L(z,t) = V_0(t)[1+\cos(2kz)]/2, \tag{4}$$

where $V_0(t)$ is the optical potential's amplitude which varies in time, and $k \equiv (2\pi/\lambda_{\rm ph})\sin(\theta/2)$ is the wave vector of the optical lattice, $\lambda_{\rm ph}$ being the wavelength of light. It is often convenient to discuss the depth of the optical potential in units of the recoil energy $E_R = (2\pi\hbar/\lambda_{\rm ph})^2/(2m)$, which is the kinetic energy gained by an atom when it absorbs a photon from the optical lattice.

Finally, the description of the mean-field dynamics of the condensate is based on the 3D time-dependent GPE,

$$i\hbar\frac{\partial}{\partial t}\Psi(\mathbf{r},t) = [\hat{p}^2/2m + V(\mathbf{r},t) + NU_0|\Psi|^2]\Psi, \tag{5}$$

where $V(\mathbf{r},t) = V_M(\mathbf{r}) - mgz + V_L(z,t)$ is the full potential (the second term is the gravitational potential), $\hat{p}^2/2m$ is the kinetic-energy operator, $U_0 = 4\pi a_0\hbar^2/m$ is the atom-atom interaction strength that is proportional to the s-wave scattering length a_0, and N is the total number of atoms. Note that, according to Eq. (3), the full potential can be written as

$$V(\mathbf{r},t) \equiv V_z(z,t) + V_\perp(\mathbf{r}_\perp), \quad \text{with} \quad V_\perp(\mathbf{r}_\perp) \equiv \tfrac{1}{2}m\omega_\perp^2(x^2+y^2). \tag{6}$$

Equation (5) can be rewritten, in terms of characteristic diffraction and nonlinear time scales $t_{\rm DF}$ and $t_{\rm NL}$, as follows [9,10]:

$$\frac{\partial\Psi}{\partial t} = i\left[\frac{r_{\rm TF}^2}{t_{\rm DF}}\nabla^2 - V(\mathbf{r},t)/\hbar - \frac{1}{t_{\rm NL}}\frac{|\Psi|^2}{|\Psi_m|^2}\right]\Psi. \tag{7}$$

Here, the diffraction time $t_{\rm DF} \equiv 2mr_{\rm TF}^2/\hbar$, with $r_{\rm TF} = \sqrt{2\mu/(m\bar{\omega}^2)}$ and $\bar{\omega} = (\omega_z\omega_\perp^2)^{1/3}$, and the nonlinear time $t_{\rm NL} \equiv (G|\Psi_m|^2/\hbar)^{-1} = (\mu/\hbar)^{-1}$ can be expressed in terms of the chemical potential μ, where $|\Psi_m|$ is the maximum magnitude of Ψ [9]. Another useful length scale is $r_{{\rm TF},z} = \sqrt{2\mu/(m\omega_z^2)}$, i.e., the TF radius in the z direction. This is the size of a TF wave function in the z direction for the harmonic potential $m\omega_z^2 z^2/2$.

III. THE SEMICLASSICAL APPROXIMATION

We consider a semiclassical approach based on the Thomas-Fermi approximation for a 3D BEC wave function in a cylindrically symmetric potential. Our treatment is broken up into different approaches depending upon whether the atomic gas density is high (in the classically allowed regions of the coordinate space) or low (in classically forbidden regions).

A. The classically allowed region

Inside the classically allowed region [not too close to its boundaries so that the atomic gas density, and hence, the nonlinear term in Eq. (5), remains sufficiently large], our description is based on the following ansatz for the 3D wave function $\Psi(\mathbf{r},t)$:

$$\Psi(\mathbf{r},t)=\psi(z,t)\left(\frac{G-V_\perp(\mathbf{r}_\perp)/|\psi(z,t)|^2}{G}\right)^{1/2}, \tag{8}$$

where $\psi(z,t)$ is a newly defined effective 1D wave function and

$$G\equiv NU_0=4\pi Na_0\hbar^2/m \tag{9}$$

[cf. Eq. (5)]. Note that the ansatz assumes a fairly simple relation between the squared 1D and 3D wave functions,

$$|\psi|^2=V_\perp/G+|\Psi|^2. \tag{10}$$

The ansatz (8) makes sense in the region of physical coordinates where

$$G|\psi(z,t)|^2-V_\perp(\mathbf{r}_\perp)>0. \tag{11}$$

Substituting the ansatz (8) into the 3D GPE and neglecting the transverse part of the kinetic-energy operator in the spirit of the TF approximation, we arrive at an effective 1D GPE,

$$i\hbar\frac{\partial\psi}{\partial t}=\left[\frac{1}{2m}\hat{p}_z^2+V_z(z,t)+G|\psi|^2\right]\psi, \tag{12}$$

upon neglecting terms proportional to $V_\perp$. Strictly speaking, to derive Eq. (12) we need a condition $V_\perp\ll G|\Psi|^2$, in terms of the 3D wave function. However, it will be shown below that the 1D equation (12) is a reasonable approximate model even when the terms $V_\perp$ and $G|\Psi|^2$ are of the same order of magnitude. The full TF approximation for stationary solutions to Eq. (12) can be obtained, as discussed in Sec. III D below, if one further neglects the longitudinal kinetic-energy operator $\hat{p}_z^2/2m$. We stress that ansatz (8) is *not* an exact solution of the full 3D GPE, and it cannot describe radial excitations of the BEC.

For the case of a harmonic transverse potential $V_\perp$ from Eq. (6), the above limitation (11) yields

$$r^2<r_m^2(z,t)\equiv\frac{2G}{m\omega_\perp^2}|\psi(z,t)|^2, \tag{13}$$

where r is the radial coordinate in the plane (x,y). The quantity r_m introduced in Eq. (13) may be regarded as a definition of the radius of the cigar-shaped BEC at given values of z and t. The 3D wave function $\Psi(r,t)$ is subject to the ordinary normalization condition,

$$2\pi\int_0^\infty rdr\int_{-\infty}^{+\infty}dz|\Psi(r,z,t)|^2=1. \tag{14}$$

Upon noting that the integration over r in Eq. (14) is confined to the region $r<r_m$ and substitution of the ansatz (8) into Eq. (14), we obtain a result

$$\begin{aligned}
&2\pi\int_{-\infty}^{+\infty}dz\int_0^{r_m}rdr|\Psi(r,z,t)|^2\\
&=\frac{2\pi}{G}\int_{-\infty}^{+\infty}dz\int_0^{r_m}rdr[G|\psi(z,t)|^2-m\omega_\perp^2r^2/2]\\
&\equiv\frac{\pi m\omega_\perp^2}{G}\int_{-\infty}^{+\infty}dz\int_0^{r_m}rdr(r_m^2-r^2)\\
&=\frac{\pi G}{m\omega_\perp^2}\int_{-\infty}^{+\infty}|\psi(z,t)|^4dz=1.
\end{aligned} \tag{15}$$

Thus, according to Eq. (15), the usual normalization condition for the 3D wave function, Eq. (14), generates the following *noncanonical* normalization condition for the effective 1D wave function:

$$\int_{-\infty}^{+\infty}|\psi(z,t)|^4dz=\frac{m\omega_\perp^2}{\pi G}. \tag{16}$$

We stress that this abnormal-looking condition is a direct result of the standard full normalization condition (14) and the ansatz (8) adopted for the 3D wave function.

We note that, as follows from Eq. (8), $\psi(z,t)\equiv\Psi(x=0,y=0,z,t)$, i.e., the function ψ is the particular value of the full wave function Ψ on the axis $x=y=0$ (therefore, the functions ψ and Ψ are measured in the same units). Despite the on-axis identity between the functions Ψ and ψ, the latter one does not have the interpretation as a probability amplitude for the distribution of atoms along the z axis; instead, the probability for finding a particle in the region between z and $z+dz$ (integrated in the transverse plane) is

$$\begin{aligned}
P(z)dz&=2\pi\int_0^\infty rdr|\Psi(r,z,t)|^2dz\\
&=\frac{\pi G}{m\omega_\perp^2}|\psi(z,t)|^4dz,
\end{aligned} \tag{17}$$

cf. Eqs. (15) and (16).

Recall that, in contrast to linear quantum mechanics, the normalization of the wave function ψ is important and affects physical results in nonlinear theories of the GPE type.

Indeed, the strength of the nonlinear mean-field term in Eq. (12) is determined by the maximum value of $|\psi|^2$ and is thus affected by the normalization.

B. The applicability condition for the Thomas-Fermi approximation

Getting back to the derivation of the 1D equation (12) from the underlying 3D GPE (5), we note that the neglect of the transverse kinetic energy is a crucially important assumption in the derivation. To estimate a physical conditions behind this assumption, we notice that, in the case of a cigar-shaped condensate, or a pancake-shaped condensate (where the height of the pancake is along the z axis), the transverse momentum may be estimated as $p_\perp \sim \hbar/r_m$, where r_m is the effective radius of the cigar (or height of the pancake, see below), for which the estimate (13) was obtained above. The transverse kinetic energy may be neglected in comparison with the confining (transverse) potential if $p_\perp^2/(2m) \ll m\omega_\perp^2 r_m^2/2$. The substitution of the above estimate for $p_\perp$ yields the condition

$$(m\omega_\perp)^2 r_m^4 \gg \hbar^2. \tag{18}$$

Further, we use Eq. (13) to estimate r_m, taking into account that $|\psi|^2$ can be estimated by means of the normalization condition (14),

$$|\psi|^2 \sim 1/(\pi r_m^2 L), \tag{19}$$

where L is the longitudinal size of the cigar. This eventually yields

$$r_m^4 \sim G/(m\omega_\perp^2 L), \tag{20}$$

and the substitution of Eq. (20) into Eq. (18) leads, with regard to expression (9) for G, to the final condition in the form of Eq. (1).

Typical values of the parameters for a cigar-shaped ^{87}Rb condensate are

$$N = 2\times 10^4, \quad \omega_z = 20 \text{ Hz}, \quad \omega_x = \omega_y = 100 \text{ Hz},$$
$$a_0 = 5.017 \text{ nm}. \tag{21}$$

Substitution of these values into Eq. (1) yields the following limitation on the length of the cigar: $L \ll 1$ mm, which is satisfied in experimentally realistic configurations. On the other hand, the assumption that the cigar is strongly stretched in the z direction implies an inequality $r_m \ll L$. Making use of relation (20), the latter condition can be cast in a final form $L \gg 1$ μm. For the parameters in Eq. (21), we find the condition

$$1 \ \mu\text{m} \ll L \ll 1 \text{ mm}. \tag{22}$$

The actual length of the cigar, as found from the full numerical solution (see below), turns out to be very close to the 3D TF estimate, $r_{\text{TF},z} \approx 17$ μm, so condition (22) is easily met. For this example, as well as those presented below in Sec. VIII, our approximation in the classically allowed regions of the coordinate space should therefore be very accurate, and this indeed is confirmed by numerical results reported in Sec. VIII.

Similarly, for a pancake-shaped ^{87}Rb condensate with

$$N = 2\times 10^4, \quad \omega_z = 100 \text{ Hz}, \quad \omega_x = \omega_y = 20 \text{ Hz},$$
$$a_0 = 5.017 \text{ nm}, \tag{23}$$

the height of the pancake is very close to the TF length in the transverse z direction, $r_{\text{TF},z} \approx 2.4$ μm (and the TF radius in the transverse direction is $r_{\text{TF},\perp} \approx 12$ μm), so condition (1) is met in this case too.

Details of the derivation of the corresponding applicability condition (2) for the pancake case are given below at the end of Sec. VII, where we show that the condition is met for values of the parameters from Eq. (23).

C. Stationary and slowly varying cases

A stationary solution to the 3D GPE with a time-independent potential $V(\mathbf{r})$ can be approximated, in classically allowed regions, by a stationary version of the ansatz (8), $\psi(r,z,t) = \phi(z)\exp[-(i/\hbar)\mu t]$, where the function $\phi(z)$ satisfies the equation

$$-\frac{\hbar^2}{2m}\frac{d^2\phi}{dz^2} + [V_z(z) - \mu]\phi + G\phi^3 = 0 \tag{24}$$

following from Eq. (12).

For problems with a slow time variation, we can consider an instantaneous eigenstate of the nonlinear time-dependent GPE equation. Adiabatically varying potentials $V_z(z,t)$ can be treated by calculating the instantaneous chemical potential and quasistationary wave function $\phi(z;t)$ in the instantaneous external potential, and then forming the full time-dependent solution as

$$\psi(r,z,t) = \phi(z;t)\exp\left[-(i/\hbar)\int_0^t dt'\,\mu(t')\right]. \tag{25}$$

Strictly speaking, the noncanonical normalization condition (16), unlike the canonical (quadratic) one, is not compatible with the full time-dependent effective 1D GPE (12). However, there is no problem with the compatibility in the case of the adiabatically slow evolution.

D. Full Thomas-Fermi approximation in the classically allowed region

The full 3D TF approximation can be recovered if we apply the TF approximation directly to the 1D equation (12), neglecting the kinetic-energy operator in it, so that the solution will be

$$\psi(z,t) = \sqrt{\frac{\mu - V_z(z,t)}{G}}\exp\left[-\frac{i}{\hbar}\int_0^t dt'\,\mu(t')\right]. \tag{26}$$

According to Eq. (8), this yields the full 3D TF wave function,

$$\Psi(\mathbf{r},t)=\left(\frac{\mu-V_\perp(\mathbf{r})_\perp-V_z(z,t)}{G}\right)^{1/2}\exp\left[-\frac{i}{\hbar}\int_0^t dt'\,\mu(t')\right]. \tag{27}$$

Substituting Eq. (26) into the noncanonical normalization condition (16) yields

$$\int_{-\infty}^{+\infty}[\mu(t)-V_z(z,t)]^2dz=Gm\omega_\perp^2/\pi, \tag{28}$$

where the region of integration over z is restricted by the condition $\mu(t)-V_z(z,t)>0$. Hence, the normalization condition (28) determines the chemical potential $\mu(t)$. Note that the condition (28) is equivalent to the usual form of the condition which determines the chemical potential in the framework of the TF approximation applied to the full 3D equation (5):

$$\frac{2\pi}{G}\int_0^\infty rdr\int_{-\infty}^{+\infty}dz[\mu(t)-V(\mathbf{r},t)]=1, \tag{29}$$

where the integration is performed over the region in which $\mu(t)-V(\mathbf{r},t)>0$. Performing the algebra, we arrive at the usual expression for the chemical potential in the static harmonic 3D potential (without an optical component):

$$\mu=\tfrac{1}{2}[15G/(4\pi)]^{2/5}(m\bar{\omega}^2)^{3/5}.$$

Finally, for any potential $V_z(z)$ (and the harmonic potential $V_\perp$), the effective probability density defined by Eq. (17) takes the following form in the TF approximation:

$$P_{\mathrm{TF}}(z)=\frac{\pi}{m\omega_\perp^2 G}|\mu-V_z(z)|^2 \tag{30}$$

in the region where $\mu-V_z(z)>0$; otherwise, $P_{\mathrm{TF}}(z)=0$.

E. Classically forbidden regions

In classically forbidden regions, the density of atoms is small, therefore the nonlinear term in the GPE may be dropped, so that it becomes tantamount to the ordinary quantum-mechanical Schrödinger equation, hence we adopt the following product ansatz for $\Psi(\mathbf{r},t)$:

$$\Psi(\mathbf{r},t)=\psi(z,t)\exp(-r_\perp^2/2R_\perp^2-i\omega_\perp t/2), \tag{31}$$

where the transverse squared radius is $R_\perp^2=\hbar/m\omega_\perp$. We stress that the Gaussian approximation for the transverse part of the ansatz (31) is appropriate, unlike in the classically allowed region, as the equation is effectively linear in the present case. Upon substituting Eq. (31) into the linearized GPE, it is straightforward to obtain an effective 1D linear Schrödinger equation,

$$i\hbar\frac{\partial\psi(z,t)}{\partial t}=\left[\frac{1}{2m}\hat{p}_z^2+V_z(z,t)\right]\psi. \tag{32}$$

Quite naturally, Eq. (32) is equivalent to Eq. (12) inside the classically forbidden region, as in this region the nonlinear term in Eq. (12) is negligible.

IV. MATCHING CONDITIONS

Equation (12) or (7) can be rewritten in the following form by rescaling t, z, and ψ:

$$iu_t+\tfrac{1}{2}u_{zz}-U(z,t)u-\gamma|u|^2u=0, \tag{33}$$

where $\gamma>0$ is a properly normalized nonlinear coupling strength. A solution to Eq. (33) is sought for as

$$u(z,t)=v(z;t)\exp\left(-i\int_0^t dt'\,\mu(t')\right), \tag{34}$$

with a real chemical potential $\mu(t)$ and a real function $v(z;t)$, cf. Eq. (25). Here, the time dependence of $U(z,t)$ is presumed to be slow enough, and $v(z;t)$ satisfies a quasistationary equation

$$[\mu(t)-U(z,t)]v+\frac{1}{2}\frac{d^2v}{dz^2}-\gamma v^3=0. \tag{35}$$

As in the ordinary semiclassical form of quantum mechanics, it is necessary to match the approximations for the wave function across the classical turning point, which separates the classically allowed and forbidden regions in the 1D space. As well as in linear quantum mechanics, the wave function in the latter region will be taken in the WKB approximation, see Eq. (36) below. However, a crucial difference from the standard theory is that the wave function in the classically allowed area is taken not in the corresponding version of the WKB approximation, but rather in the TF form. This, of course, drastically changes the matching problem (see also Ref. [8]).

Deeply under the barrier, i.e., for large positive values of the potential $U(z)$, the density of particles is small, hence, as it was already mentioned above, the nonlinear term in Eq. (35) may be dropped, and a solution may be presented in the standard semiclassical (WKB) approximation,

$$v(z)=\frac{C}{[2\{U(z)-\mu\}]^{1/4}}\exp\left[-\int_{z_0}^z\sqrt{2\{U(z')-\mu\}}dz'\right], \tag{36}$$

where, for definiteness, we choose z_0 as the classical turning point, at which $U(z_0)=\mu$, and C is (for the time being) an arbitrary real constant (because C is arbitrary, z_0 may indeed be chosen arbitrarily). It is also assumed that the classically forbidden region is located at $z>z_0$, i.e., to the right of the turning point. As usual, the WKB approximation (36) is not valid too close to the turning point.

On the other hand, the solution inside the classically allowed region ($z<z_0$), not too close to the turning point, is taken in the usual TF approximation as described above, cf. Eq. (26):

$$v_{\mathrm{TF}}=\sqrt{\frac{\mu-U(z)}{\gamma}}. \tag{37}$$

Note that, unlike the WKB solution (36), the TF approximate solution (37) does not contain any arbitrary constant.

Now we need to match the two approximations (36) and (37) across the turning point, in the vicinity of which both approximations are not applicable, the eventual objective being to find the constant C in Eq. (36). Following the usual quantum-mechanical approach, one can cast the matching problem into a standard form, expanding the potential in the vicinity of the turning point,

$$\mu-U(z)\approx F_0(z-z_0), \tag{38}$$

where F_0 is the value of the potential force at the turning point (in the present case, $F_0<0$). The accordingly modified version of Eq. (35) is

$$\frac{d^2v}{dz^2}+F_0(z-z_0)v-2\gamma v^3=0,$$

which is transformed into a normalized form

$$\frac{d^2w}{d\xi^2}=\xi w+2w^3 \tag{39}$$

by means of rescalings

$$\xi\equiv(2|F_0|)^{1/3}(z-z_0),\quad v\equiv\frac{(2|F_0|)^{1/3}}{\sqrt{\gamma}}w. \tag{40}$$

Equation (39) is a particular case of a classical equation known as the Painlevé transcendental of the second type. The full form of this equation (a standard notation for which is $\mathrm{P_{II}}$) is

$$\frac{d^2w}{d\xi^2}=\xi w+2w^3+\alpha,$$

cf. Eq. (39), where α is an arbitrary real parameter; in the present case, $\alpha\equiv 0$. The use of the expansion (38) and simplified equation (39) for matching different asymptotic solutions of an equation equivalent to Eq. (35) was proposed, in a context different from BEC, in Ref. [11] (however, the asymptotic form of the solution inside the classically allowed region, for which the analysis was done in Ref. [11], was different from Eq. (37): it corresponded to a nonlinear wave function oscillating in space, rather than to the TF case). Here, it is necessary to find a solution to Eq. (39) with the property that it takes the asymptotic forms

$$w\approx\sqrt{-\xi/2}\ \text{ and }\ w\approx\frac{\tilde{C}}{\xi^{1/4}}\exp\left(-\frac{2}{3}\xi^{3/2}\right) \tag{41}$$

at $\xi\to-\infty$ and $\xi\to+\infty$, respectively, in accordance with Eqs. (37) and (36). The actual problem is to find a value of the universal numerical constant $\tilde{C}$ in Eqs. (41) from matching the solution to its uniquely defined asymptotic form at $\xi\to-\infty$.

As mentioned above, this matching problem is different from its counterpart in ordinary (linear) quantum mechanics. An *exact solution* to this problem is available in the mathematical literature (see Ref. [12] and references to original works therein). The final result of the analysis is

$$\tilde{C}=\frac{1}{2\sqrt{\pi}}\approx 0.282. \tag{42}$$

Using this exact result, and undoing the rescalings (40), we obtain the value of the constant C in the WKB solution (36):

$$C=\tilde{C}\sqrt{\frac{2|F_0|}{\gamma}}\equiv\sqrt{\frac{|F_0|}{2\pi\gamma}}. \tag{43}$$

With the relation (43), the WKB expression (36) for the wave function under the barrier is completely defined. Of course, the result presented in the form (43) also applies when the classically forbidden region is located to the left (rather than to the right) of the classical turning point.

This result for the matching problem applies as well to the case of the adiabatically slow variation of the parameters, e.g., when F_0 slowly varies as a function of time (or when γ changes with time due to the variation of the trap potential with time). The result does not apply to the case of a vertical potential wall (when, formally, $F_0=\infty$). However, in this case, the solution is almost trivial. Indeed, assume that at the point $z=0$ there is a jump of the potential from a large negative value U_- inside the well ($z<0$) to a large positive value U_+ inside the classically forbidden region ($z>0$). Then, in the allowed region, the TF solution in the form $v=\sqrt{(\mu-U_-)/\gamma}$ is valid everywhere up to the turning point, the exact solution in the forbidden region is

$$v=C\exp[-\sqrt{2(U_+-\mu)}z],$$

and the constant C is immediately found from the continuity condition, $C=\sqrt{(\mu-U_-)/\gamma}$.

V. MOMENTUM DISTRIBUTION

The approach developed above can be naturally applied to calculate the distribution of values of the longitudinal momentum p in a given quantum state $|\Psi\rangle$, which can be measured in a direct experiment. The distribution is determined by the scalar product

$$\mathcal{P}(p)=|\langle p|\Psi\rangle|^2, \tag{44}$$

where, up to a normalization factor,

$$\langle p|=\exp\left(\frac{-ipz}{\hbar}\right) \tag{45}$$

is the conjugate eigenfunction of the momentum operator. Thus, according to Eq. (44), to determine the momentum distribution in the z direction we need to calculate nothing

else but the 1D Fourier transform of the 3D wave function (8), additionally integrated in the transverse direction [the scalar product in Eq. (44) assumes, of course, the full 3D integration]:

$$\langle p|\Psi\rangle = 2\pi \int_{-\infty}^{+\infty} dz\, \exp\left(\frac{-ipz}{\hbar}\right) \int_0^{\infty} \Psi(r_\perp, z, t) r_\perp dr_\perp, \tag{46}$$

where the multiplier 2π is generated by the angular integration in the transverse plane.

Substituting the expression (8) for Ψ inside the classically allowed region into (46), the integration over $r_\perp$ is confined to the interval $0<r_\perp<r_m$, where $r_m^2(z,t)$ is the same as defined above by Eq. (13). Taking into account the form of the transverse potential (6), we arrive at an expression

$$\begin{aligned}\langle p|\Psi\rangle &\approx 2\pi \int_{-\infty}^{+\infty} dz \exp\left(\frac{-ipz}{\hbar}\right) \psi(z,t) \\ &\times \int_0^{r_m} \left(\frac{G - V_\perp(\mathbf{r}_\perp)/|\psi(z,t)|^2}{G}\right)^{1/2} r_\perp dr_\perp \\ &= 2\pi \int_{-\infty}^{+\infty} r_m^2 dz \exp\left(\frac{-ipz}{\hbar}\right) \\ &\times \psi(z,t) \int_0^1 \sqrt{1-\rho^2}\rho d\rho,\end{aligned} \tag{47}$$

where $\rho \equiv r_\perp / r_m$. Further, using an elementary formula $\int_0^1 \sqrt{1-\rho^2}\rho d\rho = 1/3$ and the expression (13) for r_m, we obtain from Eq. (47),

$$\langle p|\Psi\rangle = \frac{4\pi}{3} \frac{G}{m\omega_\perp^2} \int_{-\infty}^{+\infty} dz \exp\left(\frac{-ipz}{\hbar}\right) \psi(z,t)|\psi(z,t)|^2, \tag{48}$$

which is the final result: Eq. (48) tells us that the amplitude $\langle p|\Psi\rangle$ of the probability distribution, which determines the probability as per Eq. (44), is

$$\langle p|\Psi\rangle = \frac{4\pi(2\pi)^{1/2}}{3} \frac{G}{m\omega_\perp^2} \mathcal{F}\{\psi|\psi|^2\}(p/\hbar), \tag{49}$$

where $\mathcal{F}$ is the symbol of the Fourier transform

$$\mathcal{F}\{f\}(\omega) \equiv \frac{1}{(2\pi)^{1/2}} \int_{-\infty}^{+\infty} \exp(-i\omega t) f(t) dt. \tag{50}$$

Inside the classically forbidden region, the usual quantum-mechanical expressions for the momentum distribution apply.

Expectation values of operators involving only the longitudinal momentum can be computed as follows, if we neglect a contribution from classically forbidden regions. Suppose we have an operator $\mathcal{O}(p)$, such as, for instance, p itself or the kinetic energy $p^2/(2m)$. Then, the expectation value of the operator $\mathcal{O}(p)$ is given by

$$\langle \Psi|\mathcal{O}(p)|\Psi\rangle = \int_{-\infty}^{+\infty} dp \mathcal{O}(p) |\langle p|\Psi\rangle|^2. \tag{51}$$

The expression (49) should be then substituted for $\langle p|\Psi\rangle$ in Eq. (51).

VI. THE CONDENSATE WITH VORTICITY

The above consideration can be generalized for a case when the condensate inside the cylindrically symmetric region is given vorticity, so that the wave function has the form

$$\Psi(r,z,t) = \exp(il\theta)\Phi(r,z,t), \tag{52}$$

where θ is the angular coordinate in the transverse plane and l is the vorticity quantum number. The ansatz (8) is then replaced by

$$\begin{aligned}\Psi(r,z,t) &= \exp(il\theta) G^{-1/2} \\ &\times \sqrt{G|\psi_l(z,t)|^2 - \left(m\omega_\perp^2 r^2/2 + \frac{\hbar^2 l^2}{2mr^2}\right)}.\end{aligned} \tag{53}$$

The corresponding normalization condition replacing Eq. (14) takes the form

$$2\pi \int_{-\infty}^{+\infty} dz \int_{r_{\min}}^{r_m} r dr |\Psi(r,z,t)|^2 = 1, \tag{54}$$

where now

$$r_m^2 = \frac{1}{m\omega_\perp^2}\left[G|\psi_l|^2 + \sqrt{G^2|\psi_l|^4 - (l\hbar\omega_\perp)^2}\right], \tag{55}$$

$$r_{\min}^2 = \frac{1}{m\omega_\perp^2}\left[G|\psi_l|^2 - \sqrt{G^2|\psi_l|^4 - (l\hbar\omega_\perp)^2}\right]. \tag{56}$$

The corresponding 1D GPE equation for $\psi_l(z,t)$ is

$$i\hbar \frac{\partial \psi_l}{\partial t} = \left[\frac{1}{2m}\hat{p}_z^2 + V_z(z,t) + G|\psi_l|^2\right]\psi_l.$$

Finally, the substitution of the expressions (53), (55), and (56) into Eq. (54) yields, after a straightforward calculation of the integral over the radial variable r, an effectively 1D normalization condition in a complicated form, which is a generalization of the above noncanonical normalization condition (16) corresponding to $l=0$:

$$\begin{aligned}\int_{-\infty}^{+\infty} dz \Bigg[&\frac{G|\psi_l(z)|^2\sqrt{G^2|\psi_l(z)|^4 - (l\hbar\omega_\perp)^2}}{m^2\omega_\perp^4} \\ &- \left(\frac{\hbar l}{m\omega_\perp}\right)^2 \ln\left(\frac{2G^2|\psi_l(z)|^4}{(l\hbar\omega_\perp)^2} - 1\right. \\ &\left. + \frac{2G|\psi_l(z)|^2}{l\hbar\omega_\perp}\sqrt{\frac{G^2|\psi_l(z)|^4}{(l\hbar\omega_\perp)^2} - 1}\right)\Bigg] = \frac{2G}{\pi m\omega_\perp^2}.\end{aligned} \tag{57}$$

Note that, with $l=0$, this result indeed reduces to Eq. (16). A consequence of Eq. (57) is that $|\psi_l(z)|^2$ cannot take values smaller than $(|\psi_l(z)|^2)_{\min}=(l\hbar\omega_\perp)/G$. Furthermore, from Eq. (53) it is clear that the condition $G|\psi_l(z,t)|^2-[m\omega_\perp^2 r^2/2+(\hbar l/r)^2/(2m)]>0$ must be satisfied for the ansatz (53) to be valid.

VII. THE BROKEN-SYMMETRY CONDENSATE

As mentioned in the Introduction, the approach developed above can be extended to the case when the cylindrical symmetry about the z axis is broken by a nonaxisymmetric potential $V_{xy}(x,y)$. In this case, essentially the same ansatz as given by Eq. (8) may be employed if the potential is harmonic in z. Accordingly, we take the transverse potential as $V_\perp(z)=(1/2)m\omega_\perp^2 z^2$, cf. Eq. (6), and an ansatz in the form

$$\Psi(\mathbf{r},t)=\psi(x,y,t)\left(\frac{G-m\omega_\perp^2 z^2/2|\psi(x,y,t)|^2}{G}\right)^{1/2}. \quad (58)$$

Note that the interpretation of the function $\psi(x,y,t)$ is similar to that of the function $\psi(z,t)$ in the ansatz (8): it coincides with the full 3D wave function $\Psi(x,y,z,t)$ at $z=0$. Substitution of Eq. (58) into the 3D normalization condition (14) and straightforward integration in the z direction, which is actually limited to the interval

$$0<z^2<z_m^2\equiv\frac{2G}{m\omega_\perp^2}|\psi(x,y,t)|^2 \quad (59)$$

[cf. Eq. (13)], yields a result

$$\int_{-\infty}^{+\infty}\int_{-\infty}^{+\infty}|\psi(x,y)|^3dx\,dy=\frac{3}{4}\sqrt{\frac{m\omega_\perp^2}{2G}}, \quad (60)$$

cf. Eq. (16). This is another example of the noncanonical normalization condition, which is generated by the reduction in the effective space dimension. As for the effective 2D GPE generated by the ansatz (58), it has the usual form

$$i\hbar\frac{\partial\psi(x,y,t)}{\partial t}=\left[\frac{1}{2m}(\hat{p}_x^2+\hat{p}_y^2)+V_{xy}(x,y,t)\right]\psi, \quad (61)$$

cf. Eq. (12) [a formal condition under which Eq. (61) can be derived from the 3D equation (5) is $m\omega_\perp^2 z^2\ll|\psi(x,y,t)|^2$].

We do not consider the problem of matching the wave function in the classically allowed and forbidden regions in the framework of the 2D equation (61), as the WKB approximation for the classically forbidden region is itself problematic in the 2D case. In fact, this approximation was only elaborated for the 2D motion in an axially symmetric field [7], which does not correspond to the situation of interest in the present context [the axial symmetry in the (x,y) plane will be destroyed by the optical lattice].

Finally, to estimate the applicability of the TF approximation, i.e., the possibility to neglect the transverse kinetic energy (along the height of the pancake) in the course of the derivation of the 2D equation (61), we notice that this can be carried out following the lines of the analysis presented above for the cigar-shaped condensate (where the pancake-shaped case was mentioned too), with the only difference that the normalization condition in the present case yields an estimate for the squared wave function different from that given by Eq. (19): $|\psi|^2\sim 1/(\pi R^2 z_m)$, where z_m is the effective transverse size of the pancake condensate, according to Eq. (59), and R is a characteristic radius of the pancake. Accordingly, the final estimate for the transverse size is different from that given by Eq. (20) for the cigar:

$$z_m^3\sim\frac{G}{m\omega_\perp^2}R^{-2}. \quad (62)$$

The substitution of Eq. (62) into the condition that the transverse kinetic energy must be much smaller than the confining potential yields the eventual result (2).

For example, if the same values of physical parameters as given in Eq. (23) are adopted in the present case, the condition (2) imposes the following limitation on the pancake's radius: $R\lesssim 0.01$ mm. As well as in the case of the cigar, another condition must be added, to guarantee that the radius R is much larger than the transverse size z_m (i.e., the condensate is indeed shaped like a pancake). Making use of Eq. (62) and again taking the values of the parameters from Eq. (21), one can cast the latter condition in the form $R\gg 1$ μm. Thus, the present approach applies to the pancake-shaped condensates if 1 $\mu\text{m}\ll R\lesssim 10$ μm. Although this condition is essentially more restrictive than its counterpart for the cigar-shaped condensates, it can be implemented in the experiment (in fact, one may expect that the pancake configuration will be created with a larger number of atoms than the cigar, then the above conditions will assume a less restrictive form). The TF length in the z direction is $r_{\text{TF},z}\approx 2.4$ μm, and the TF-radius $R_{\text{TF},\perp}\approx 12$ μm, and these are very close to the numerically computed lengths, so our condition (2) is met. If, for other values of the physical parameters, the conditions are not met, the approach developed in Refs. [4] or [5] may be applicable.

VIII. NUMERICAL RESULTS

For the numerical solution of Eqs. (5) and (12), we used the standard split-step operator method [13]. The computational grids had 65 536 and $32\times 32\times 2048$ points for the 1D and 3D cases, respectively, with spatial steps $\Delta h_z\approx 0.0002 r_{\text{TF},z}$ for the 1D geometry, and $\Delta h_x=\Delta h_y\approx 0.13\, r_{\text{TF}}$ and $\Delta h_z\approx 0.005 r_{\text{TF}}$ for the 3D case. We used two different methods for finding stationary solutions to GPE (24), and to its 3D counterpart: the first technique was an imaginary-time version of the split-step operator method [9], and the second is the standard finite-difference method used to solve a two-point boundary-value problem [14]. It is important to note that, by treating Eq. (24) as a two-point boundary problem, the initial conditions must include the eigenvalue μ. This will, generally, give an unphysical solution for ϕ, since the normalization condition will not be met. By gradually changing the value of μ, and redetermining the wave function of the nonlinear GPE using the finite-difference method, we can follow the surface of solutions to Eq. (24) until a physical solution is obtained.

Numerically, we find the imaginary time split-step relax-

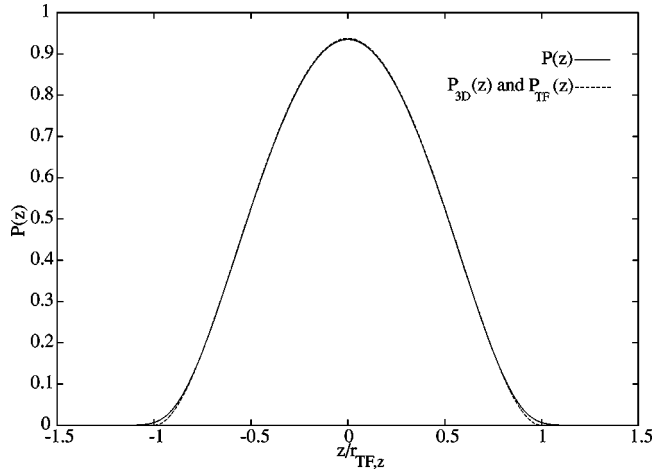

FIG. 1. The probability $P(z)$ for the 3D harmonic potential vs $z/r_{\mathrm{TF},z}$, as found numerically using Eq. (7), and $P_{\mathrm{TF}}(z)$ vs $z/r_{\mathrm{TF},z}$, as calculated using Eq. (30). The probability $P_{3\mathrm{D}}(z)$ found from the stationary version of the full 3D equation (see the text) cannot be discerned, as it lies on top of $P_{\mathrm{TF}}(z)$.

ation method painfully difficult to converge in 3D for the cigar-shaped geometry that we used in the calculations, both with and without the optical potential. The finite-difference two-point boundary-value method appears to be more efficient. For dynamical simulations, however, we used only the split-step method.

We first consider the case when only the harmonic potential is present; the action of an optical potential on the trapped BEC will be considered below. In the calculations, we take a ^{87}Rb condensate with $N=10^6$ atoms, $\omega_z=20$ Hz, $\omega_x=\omega_y=100$ Hz, and $a_0=5.017$ nm. For the parameters used in the calculation, the TF radius in the z direction is $r_{\mathrm{TF},z}=36.35\ \mu$m, in the x,y directions $r_{\mathrm{TF},\perp}=7.27\ \mu$m, and the chemical potential is $\mu=1.507\times10^{-30}$ J. The applicability condition (1) definitely holds in this case.

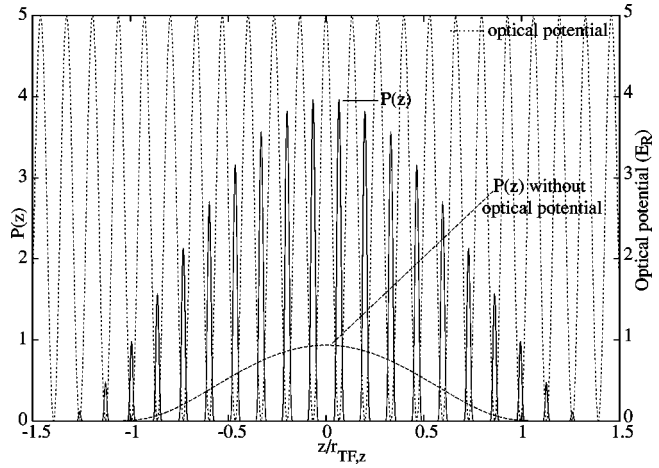

FIG. 2. The probability $P(z)$ for the combination of the 3D harmonic and optical potentials vs $z/r_{\mathrm{TF},z}$, as found numerically using Eq. (7). For comparison, the probability $P(z)$ without the optical potential, and the optical potential itself are also shown.

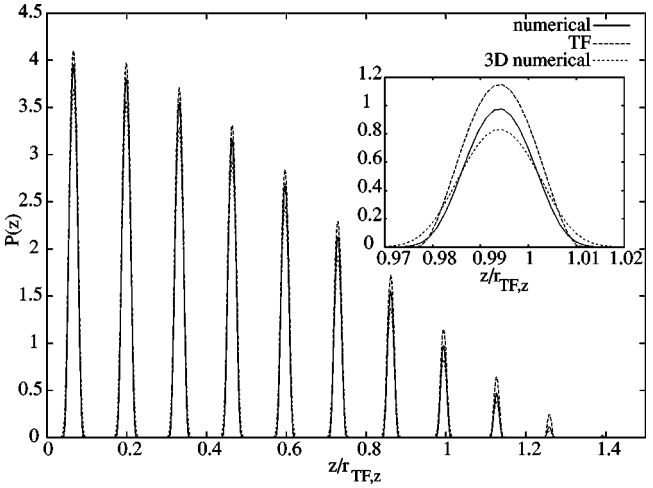

FIG. 3. The probability distributions $P(z)$, $P_{3D}(z)$, and $P_{\mathrm{TF}}(z)$ vs $z/r_{\mathrm{TF},z}$ for the combination of the 3D harmonic and optical potentials. The inset is an enlargement of the region near $z/r_{\mathrm{TF},z}=1$.

Figure 1 shows the probability $P(z)$ versus z, as calculated using Eq. (7). Also shown is the probability $P_{\mathrm{TF}}(z)$ as obtained from the full TF approximation based on Eq. (30), and a probability $P_{3D}(z)$ found from the numerical solution of the full 3D GPE. The curve obtained from the 3D GPE lies on top of the TF curve, being nearly indiscernible from it (it is no surprise that TF is a good approximation for 10^6 Rb atoms in a harmonic trap). Clearly, the comparison of the $P(z)$ found by means of the approximation developed above with the TF and full 3D results is excellent. A slight deterioration occurs in the region where the density is low.

Figure 2 shows the probability distribution for the same harmonic potential as in Fig. 1, but with an added optical-lattice potential as given by Eq. (4), with the wavelength $\lambda_{\mathrm{ph}}=840$ nm, relative angle $\theta=10°$ between the two light beams, and the constant amplitude $V_0=5E_R$. For this wavelength, the recoil energy $E_R=\hbar^2(2\pi/\lambda)^2/(2m)=2.15\times10^{-30}$ J, so the optical potential's strength is about 1.4 times the value of the chemical potential in the absence of the optical lattice. In the presence of the optical lattice, the

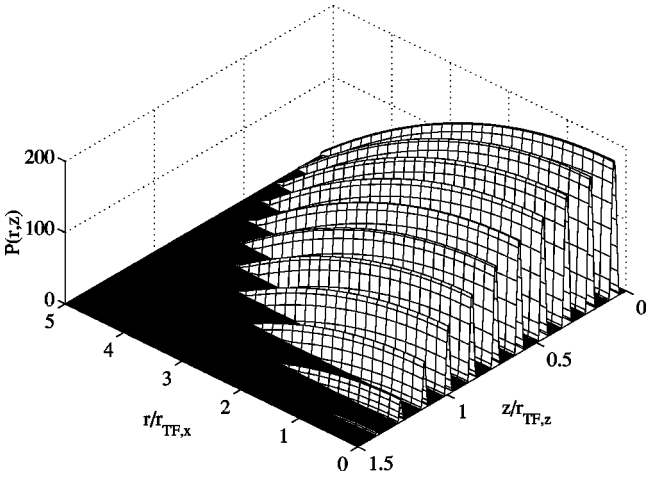

FIG. 4. The probability $|\Psi(\mathbf{r})|^2$ vs x and z.

chemical potential is calculated to be 3.15×10^{-30} J (slightly more than twice the chemical potential without the optical lattice). Also shown in Fig. 2 is the optical potential $V_L(z)$, and $P(z)$ determined without the optical lattice (as in Fig. 1). As is seen from the figure, the optical potential squeezes the atomic density out to larger z; it also squeezes it out to larger x and y, see below.

Figure 3 shows the comparison of $P(z)$ with $P_{\rm TF}(z)$ and $P_{3D}(z)$, where $P_{\rm TF}(z)$ is calculated using Eq. (30), and with $P_{3D}(z)$ as obtained by solving the stationary 3D GPE. The TF result still provides an adequate description, despite the fact that the kinetic energy is more important in this case than in the case without the optical potential. Hence we conclude that the kinetic energy remains much less significant than the potential and the mean-field energy in this case. Our method produces results closer to the 3D result than the TF. The kinetic energy does broaden the wave function in each optical well, hence peaks of the wave functions are lower than in the TF approximation, as evident in Fig. 3. Note, however, that our method, being based on a TF-type approximation in the transverse dimension, restricts the diffusion of the wave function due to the kinetic energy to the z direction (but the wave function is definitely squeezed into the transverse dimension due to the optical potential and the mean field—see below). The inset in the figure is an enlargement of the region near $z/r_{{\rm TF},z}=1$.

Figure 4 shows $|\Psi(\mathbf{r})|^2$ versus r and z. A striking aspect of this figure is the extent to which the wave function is squeezed out to larger r in the presence of the optical potential. Without this potential, the size of the wave function in r is $r_{{\rm TF},x}$ $(=r_{{\rm TF},y})$, but now it is squeezed out to about $5\,r_{{\rm TF},x}$. The size of the wave function in the radial direction depends upon z, as does the extent of the squeezing in r. The distribution of $|\Psi(\mathbf{r})|^2$ versus r and z, as produced by the stationary 3D GPE, is similar to that obtained by our method.

Finally, in Fig. 5 we show results of a dynamical calculation in which we varied the optical potential as a function of time, so that the peak strength of the optical potential depended on time as $V_0(t)=5E_R\exp(-[(t-t_F)/\sigma]^2)$, with $t_F=1.12$ ms and $\sigma=t_F/2=0.56$ ms. The calculated probability distribution $P(z,t)$ is shown at four different times, viz., at $t=0$ before the optical potential is ramped up, at $t=t_F/5$ when the optical potential is still rather small, at $t=t_F/2$ when the optical potential is somewhat less than 0.4 times its final value of $5E_R$, and at $t=t_F$ when $V_0(t_F)=5E_R$. The dynamics are initially adiabatic, but, clearly, by the final time, $t_F=1.12$ ms, the dynamics cease to be adiabatic (compare the result with the probability distribution shown in Fig. 2). The dynamics of the probability $P(z,t)$ versus z, calculated using the 3D GPE, are similar to that shown in Fig. 5.

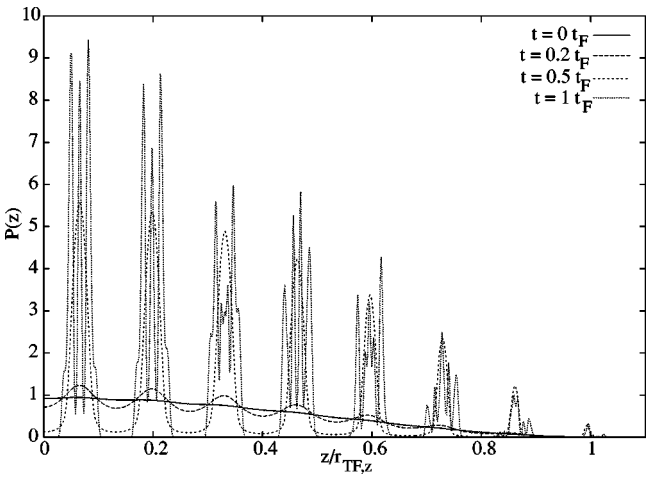

FIG. 5. The probability $P(z,t)$ vs z at four different values of time, $t=0$ $[V_0(0)=0]$, $t=t_F/5$ $[V_0(t_F/5)=0.387E_R]$, $t=t_F/2$ $[V_0(t_F/2)=1.839E_R]$, $t=t_F$ $[V_0(t_F)=5E_R]$.

IX. SUMMARY AND CONCLUSIONS

We have proposed several improvements to the semiclassical description of BECs in three dimensions. First, an ansatz that makes it possible to reduce the corresponding 3D GPE to an effectively 1D equation in the cylindrically symmetric case was put forward. An interesting feature of this approach is that the corresponding 1D normalization condition, which follows from the standard normalization condition in the full 3D description, takes a noncanonical form, containing the fourth power of the 1D wave function, rather than its square. Also noncanonical is an expression for the probability density of the distribution of the 1D momentum. These results were further extended to cases when the BEC has vorticity, and when cylindrical symmetry is absent; these cases yield additional examples of noncanonical normalization conditions, sometimes of quite a complicated form. For both cases with the imposed and broken cylindrical symmetry, explicit conditions for the applicability of the effective low-dimensional equations were produced.

Another result, obtained in the framework of the effectively 1D description, is an explicit matching formula between the TF approximation valid inside the classically allowed region, and the exponentially vanishing WKB approximation valid inside the classically forbidden region. Here, an exact solution to a problem found long ago in an abstract mathematical context determines the arbitrary constant in front of the exponentially decaying WKB wave function.

To verify the validity of analytical approximations developed in this work, we have performed direct numerical calculations of bound states and of dynamics in a time-dependent potential, and compared the probability distributions obtained with full 3D results. The comparison shows that the analytical approximations are quite accurate.

ACKNOWLEDGMENTS

We appreciate useful discussions with M. J. Ablowitz and L. Salasnich. This work was supported, in a part, by Grant Nos. 1998-421 and 1999-459 from the U.S.-Israel Binational Science Foundation, the Israel Science Foundation (Grant No. 212/01), and the Israel Ministry of Defense Research and Technology Unit.

[1] F. Dalfovo *et al.*, Rev. Mod. Phys. **71**, 463 (1999).
[2] Y. Castin and R. Dum, Phys. Rev. Lett. **77**, 5315 (1996); **79**, 3553 (1997).
[3] Y. Japha and Y.B. Band, J. Phys. B **35**, 2383 (2002).
[4] P. Pedri *et al.*, Phys. Rev. Lett. **87**, 220401 (2001).
[5] L. Salasnich, A. Parola, and L. Reatto, Phys. Rev. A **65**, 043614 (2002).
[6] L. Salasnich, A. Parola, and L. Reatto, J. Phys. B **35**, 3205 (2002).
[7] L.D. Landau and E.M. Lifshitz, *Quantum Mechanics* (Pergamon, Oxford, 1977).
[8] T. Hyouguchi, S. Adachi, and M. Ueda, Phys. Rev. Lett. **88**, 170404 (2002).
[9] M. Trippenbach, Y.B. Band, and P.S. Julienne, Phys. Rev. A **62**, 023608 (2000).
[10] M. Trippenbach, Y.B. Band, and P.S. Julienne, Opt. Express **3**, 530 (1998).
[11] R. Haberman, Stud. Appl. Math. **57**, 247 (1977).
[12] M.J. Ablowitz and H. Segur, *Solitons and the Inverse Scattering Transform* (SIAM, Philadelphia, 1981), Sec. 3.7.d.
[13] J.A. Fleck, J.R. Morris, and M.D. Feit, Appl. Opt. **10**, 129 (1976); M.D. Feit and J.A. Fleck, *ibid.* **17**, 3390 (1978); **18**, 2843 (1979).
[14] W.H. Press *et al.*, *Numerical Recipes* (Cambridge University Press, New York, 1986).